

Article

# A New Algorithm of the FPAR Product in the Heihe River Basin Considering the Contributions of Direct and Diffuse Solar Radiation Separately

Li Li <sup>1</sup>, Yongming Du <sup>1</sup>, Yong Tang <sup>1</sup>, Xiaozhou Xin <sup>1</sup>, Hailong Zhang <sup>1</sup>, Jianguang Wen <sup>1</sup> and Qinhuo Liu <sup>1,2,\*</sup>

<sup>1</sup> State Key Laboratory of Remote Sensing Science, Institute of Remote Sensing and Digital Earth, Chinese Academy of Sciences, Beijing 100101, China; E-Mails: lili3982@163.com (L.L.); ymdushandong@foxmail.com (Y.D.); tangyong@163.com (Y.T.); xin\_xzh@sohu.com (X.X.); zhlnjnu@163.com (H.Z.); wenjg@radi.ac.cn (J.W.)

<sup>2</sup> Joint Center for Global Change Studies (JCGCS), Beijing 100875, China

\* Author to whom correspondence should be addressed; E-Mail: liuqh@radi.ac.cn; Tel./Fax: +86-10-6488-9229.

Academic Editors: Xin Li, Yuei-An Liou, Richard Müller and Prasad S. Thenkabail

Received: 22 December 2014 / Accepted: 13 May 2015 / Published: 21 May 2015

---

**Abstract:** It remains a challenging issue to accurately estimate the fraction of absorbed photosynthetically-active radiation (FPAR) using remote sensing data, as the direct and diffuse radiation reaching the vegetation canopy have different effects for FPAR. In this research, a FPAR inversion model was developed that may distinguish direct and diffuse radiation (the DnD model) based on the energy budget balance principle. Taking different solar zenith angles and diffuse PAR proportions as inputs, the instantaneous FPAR could be calculated. As the leaf area index (LAI) and surface albedo do not vary in a short periods, the FPAR not only on a clear day, but also on a cloudy day may be calculated. This new method was used to produce the FPAR products in the Heihe River Basin with the Moderate-Resolution Imaging Spectroradiometer (MODIS) LAI and surface albedo products as the input data source. The instantaneous FPAR was validated by using field-measured data (RMSE is 0.03,  $R^2$  is 0.85). The daily average FPAR was compared with the MODIS FPAR product. The inversion results and the MODIS FPAR product are highly correlated, but the MODIS FPAR product is slightly high in forest areas, which is in agreement with other studies for MODIS FPAR products.

**Keywords:** FPAR; direct radiation; diffuse radiation; radiative transfer model

---

## 1. Introduction

FPAR is the fraction of the incoming absorbed photosynthetically-active radiation (PAR) that a plant canopy absorbs for photosynthesis and growth in the 0.4–0.7 nm spectral range [1]. FPAR is a very important parameter in calculating gross primary productivity (GPP) using the light-use efficiency model. It is also used to estimate the assimilation of carbon dioxide by vegetation. FPAR can also be used as an indicator of the state and evolution of vegetation cover; this function can advantageously replace the normalized Difference Vegetation Index (NDVI).

The FPAR inversion methods generally use the relationship between FPAR and NDVI [2] or between FPAR and the Enhanced Vegetation Index (EVI) [3]. In a certain range, there is a linear relationship between FPAR and NDVI [4,5]. In the Carnegie–Ames–Stanford approach (CASA) model, for example, FPAR is calculated using the NDVI linear stretching model [5,6]. Myneni *et al.* used an empirical relationship based on NDVI as a backup algorithm for MODIS FPAR product derivation (MOD15) [1]. In the vegetation photosynthesis model (VPM) [7,8], FPAR is a function of EVI, but the difference between EVI and NDVI increases the blue band reflectivity in the EVI calculation. These empirical functions are mostly based on measured data or from the regression of large amounts of historical data. This may possibly indicate that a function gives good results only at a local scale. It has been a difficult issue to find the relationship for large-area FPAR inversion using remote sensing data. Myneni *et al.* studied the relationship of FPAR changes with soil, vegetation canopy and atmospheric parameters [6]. The relationship of FPAR and NDVI is independent of pixel heterogeneity, but sensitive to background characteristics and atmospheric and bidirectional reflectance. If the study focusses on the nadir, the influence of atmospheric and bidirectional reflectance can be ignored, even if the soil is moderately reflective and the background impact is also negligible. Therefore, Roujean *et al.* believe that the conditions for a linear relationship between FPAR and NDVI are: a solar zenith angle less than 60°, a focus on the nadir, a soil background of medium brightness and an atmospheric optical thickness at 550 nm of less than 0.65 [9]. In addition, NDVI is also affected by chlorophyll content. Dawson *et al.* found that NDVI is sensitive to the chlorophyll content of the canopy and the bottom leaves [10]. Therefore, establishing the conditions of the relationships between FPAR and all kinds of vegetation indices is very challenging. This kind of method is not universal and, coupled with the NDVI saturation phenomenon, will reduce FPAR inversion accuracy. On the other hand, some researchers have been trying to find out an FPAR expression based on the radiative transfer mechanism. The MODIS FPAR algorithm describes canopy spectral and directional characteristics based on the three-dimensional radiative transfer model [6]. Chen *et al.* also derived an expression between FPAR, surface albedo, canopy gap probability and LAI based on radiative transfer theory [11]. Tao obtained FPAR expressions combining the radiative transfer model and a geometrical optics model [12]. Fan *et al.* developed a new FAPAR-P model, which considers the effects of canopy structures, ambient radiation and multiple scattering between soil and vegetation [13]. This kind of method has a clear physical mechanism and is more universal than empirical models.

PAR on the top of the vegetation canopy can be classified into direct radiation and diffuse radiation. These two parts have different irradiation paths and intensities. Moreover, the canopy absorption of the two parts is not the same, which affects vegetation canopy GPP. Research has shown that due to the stronger transmission of diffuse radiation in the canopy and avoidance of the light-saturation phenomenon of direct radiation in the canopy leaves, photosynthesis is more efficient under the action of diffuse radiation [14–17]. Mercado *et al.* analyzed the impact of diffuse radiation on forest canopy GPP under the assumption that direct radiation can expose only sunlit leaves, but that diffuse radiation can expose both sunlit and shaded leaves [18]. The results showed that aerosols from human activities have increased the proportion of diffuse radiation and improved forest canopy GPP. He *et al.* simulated GPP using changes in total PAR and the proportion of diffuse PAR by means of the MAESTRA model [19]. The results showed that increasing the proportion of diffuse radiation can improve the absorption and utilization efficiency of incident PAR on the forest canopy. Therefore, the diffuse radiation effects on vegetation canopy GPP cannot be ignored. Direct and diffuse radiation follow different transfer paths in the vegetation canopy, making their FPAR values different.

To perform further research on the difference between direct and diffuse FPAR, it is necessary to analyze the variation characteristics of direct and diffuse FPAR. Using the SAIL (scattering by arbitrarily-inclined leaves) model, Baret *et al.* explored the effects of background spectral reflectance and canopy optical and geometrical properties on the relationship between FPAR and SVI [20]. Roujean *et al.* also used the SAIL model to simulate radiation transfer inside the canopy. Zhou *et al.* simulated FPAR using a Monte Carlo model and analyzed the influencing factors of FPAR, such as solar zenith angle and LAI [21]. Tao *et al.* also simulated FPAR based on a Monte Carlo model and analyzed the effects of soil background and leaf angle on vegetation canopy FPAR [12]. A previous study by the authors of this article used the SAIL model to simulate direct and diffuse FPAR under various weather and LAI conditions. The SAIL model is a radiation transfer model developed from the SUITS model [22]. The scattering and extinction coefficients of the SAIL canopy reflectance model are derived for the case of a fixed arbitrary leaf inclination angle and a random leaf azimuth distribution. The SAIL model includes the uniform model of G.H Suits as a special case, and its main characteristics are that canopy variables, such as leaf area index and the leaf inclination distribution function, are used as input parameters and that it provides more realistic angular profiles of directional reflectance as a function of view angle or solar zenith angle [23–25]. In the SAIL model, the proportions of direct and diffuse radiation can be changed by means of the visibility parameter. The results showed that when visibility was set to 5 km, 15 km and 30 km, the contributions of diffuse FPAR to total FPAR were 52.6%, 29.3% and 21.7%, respectively [26]. The error between total and direct FPAR was reduced with increasing visibility and increased with decreasing LAI. The maximum relative error was 13.2%. Simulation analyses revealed that direct and diffuse FPAR varied with changes in environmental variables. Especially when visibility was low, diffuse FPAR was an important part of total FPAR, and therefore, when modeling FPAR, the diffuse part cannot be ignored. Because the transmission process is different for direct and diffuse FPAR, the two must be modeled separately. This separation helps improve FPAR inversion accuracy. Li and Fang developed a look-up table method for inverse direct, diffuse and total FPAR based on a coupled soil-leaf canopy radiative transfer model (SLC), which could inverse the fraction of photosynthetically-active radiation absorbed by green elements [27]. Therefore, in this study, an FPAR inversion model was developed that distinguishes between direct and diffuse FPAR based on the

principle of the energy budget balance. MODIS LAI and surface albedo products were used as the model input data. At the end of this paper, the FPAR inversion was verified against observed data. This new method was used to produce the FPAR product in the Heihe River Basin. These regional FPAR products can be used as the input parameters of the ecological models to calculate GPP and NPP products.

## 2. Methods

According to the principle of the energy budget balance, the relationship between surface albedo and FPAR can be expressed in Equation (1):

$$(1 - \alpha) = A_{soil} + FPAR \quad (1)$$

where  $\alpha$  is the surface albedo. Therefore,  $(1 - \alpha)$  is the proportion of the radiance absorbed by the land surface, which can be divided into two parts, one is that absorbed by vegetation, namely  $FPAR$ , the other is that absorbed by soil, noted as  $A_{soil}$ .

In our proposed model, FPAR was separated into two parts, direct  $FPAR$  and diffuse  $FPAR$ , as expressed in Equation (2):

$$FPAR = (1 - k) \times FPAR_{dir} + k \times FPAR_{diff} \quad (2)$$

where  $FPAR$  is the total  $PAR$ ,  $FPAR_{dir}$  is the fraction of absorbed direct  $PAR$  reaching the top of the canopy,  $FPAR_{diff}$  is the fraction of absorbed diffuse  $PAR$  reaching the top of the canopy and  $k$  is the proportion of diffuse  $PAR$ .

Firstly, in order to distinguish direct and diffuse  $FPAR$ , instead of the surface albedo ( $\alpha$ ), the black sky albedo integrated from 400 to 700 nm ( $\alpha_b$ ) and the white-sky albedo integrated from 400–700 nm ( $\alpha_w$ ) need to be used in the model.

The derivation of the equation for calculating direct  $FPAR$  is described as follows.

The incident light can be divided into the part irradiated to the vegetation and the part irradiated to the soil. The probability of the incident light irradiating to the vegetation is  $(1 - P_{gap})$ , and the probability of the incident light irradiating to the soil is  $P_{gap}$ .  $P_{gap}$  is:

$$P_{gap} = \exp[-LAI \times \Omega(\theta_s) \times G(\theta_s) / \mu_s] \quad (3)$$

where  $\Omega(\theta_s)$  and  $G(\theta_s)$  are, respectively, the clumping index of foliage and the projection coefficient of the solar zenith angle  $\theta_s$  [11,28];  $\mu_s$  is the cosine of  $\theta_s$ .

If only considering the condition of the direct incident light absorbed by the land surface, Equation (1) can be written as Equation (4).

$$(1 - \alpha_b) = A_{soil-dir} + FPAR_{dir} \quad (4)$$

$A_{soil}$  can be expressed as:

$$A_{soil-dir} = \alpha_d \times P_{gap} \quad (5)$$

where  $\alpha_d$  is the absorptivity of the soil background.

If the multiple scattering between soil background and vegetation canopy is not considered,  $FPAR_{dir}$  can be expressed as:

$$FPAR_{dir} = \alpha_L \times (1 - P_{gap}) \quad (6)$$

where  $\alpha_L$  is the absorptivity of the vegetation canopy.

Therefore, the portion of sunlight directly absorbed by the vegetation canopy and the soil background can be expressed as:

$$(1 - \alpha_b) = \alpha_d \times P_{gap} + \alpha_{L-dir} \times (1 - P_{gap}) \quad (7)$$

If the soil absorptivity  $\alpha_d$  is  $a$  times the vegetation canopy absorptivity  $\alpha_L$ , the formulas for these can be expressed as:

$$\alpha_d = a_{dir} \alpha_{L-dir} \quad (8)$$

$$(1 - \alpha_b) = a_{dir} \times \alpha_{L-dir} \times P_{gap} + \alpha_{L-dir} - \alpha_{L-dir} \times P_{gap} \quad (9)$$

$$(1 - \alpha_b) = \alpha_{L-dir} \times [1 + (a_{dir} - 1)P_{gap}] \quad (10)$$

$$\alpha_{L-dir} = \frac{1 - \alpha_b}{[1 + (a_{dir} - 1)P_{gap}]} \quad (11)$$

$$FPAR_{dir} = \frac{(1 - \alpha_b) \times (1 - P_{gap})}{[1 + (a_{dir} - 1)P_{gap}]} \quad (12)$$

The derivation of the equation for calculating diffuse FPAR is described as follows.

The openness of the crown at the top of the canopy  $K_{open}$  is used, which describes how much of the PAR scattered by the ground passes through the crown to the top of the canopy.  $K_{open}$  can be expressed as in Equation (13) [29]:

$$K_{open} = \int_0^{\pi/2} P_{gap}(\theta) \sin 2\theta d\theta \quad (13)$$

If only considering the condition of the direct incident light absorbed by the land surface, Equation (1) can be written as Equation (14).

$$(1 - \alpha_w) = A_{soil-diff} + FPAR_{diff} \quad (14)$$

$A_{soil}$  can be expressed as:

$$A_{soil-diff} = \alpha_d \times K_{open} \quad (15)$$

If the multiple scattering between the soil background and vegetation canopy is not considered,  $FPAR_{diff}$  can be expressed as:

$$FPAR_{diff} = \alpha_{L-diff} \times (1 - K_{open}) \quad (16)$$

If only considering the condition of the diffuse incident light absorbed by the land surface, Equation (1) can be written as Equation (17).

$$(1 - \alpha_w) = \alpha_d \times K_{open} + \alpha_{L-diff} \times (1 - K_{open}) \quad (17)$$

If the soil absorptivity  $\alpha_d$  is  $a$  times the vegetation canopy absorptivity  $\alpha_L$ , the formulas for these can be expressed as:

$$\alpha_d = a_{diff} \alpha_{L-diff} \quad (18)$$

$$FPAR_{diff} = \frac{(1 - \alpha_w) \times (1 - K_{open})}{[1 + (a_{diff} - 1)K_{open}]} \quad (19)$$

Due to the frequent change of weather conditions, the diffuse PAR proportion ( $k$ ) varies throughout the day, and the solar zenith angle also changes. Therefore, the direct, diffuse and total  $FPAR$  all vary

during the day. In this paper, daily average *FPAR* can be calculated from the various input variables of solar zenith angle and the diffuse *PAR* proportion (Equation (20)):

$$FPAR = \frac{\sum_{t=0}^n (1 - k_t) \times FPAR_{dir t} + k_t \times FPAR_{diff t}}{n} \tag{20}$$

where *t* represents a given moment.

*Inversion Process*

The *FPAR* inversion of the DnD model involves many input variables, such as *LAI*, surface albedo, land cover, diffuse *PAR* proportion, date, longitude and latitude. Figure 1 shows a flowchart of the *FPAR* inversion procedure.

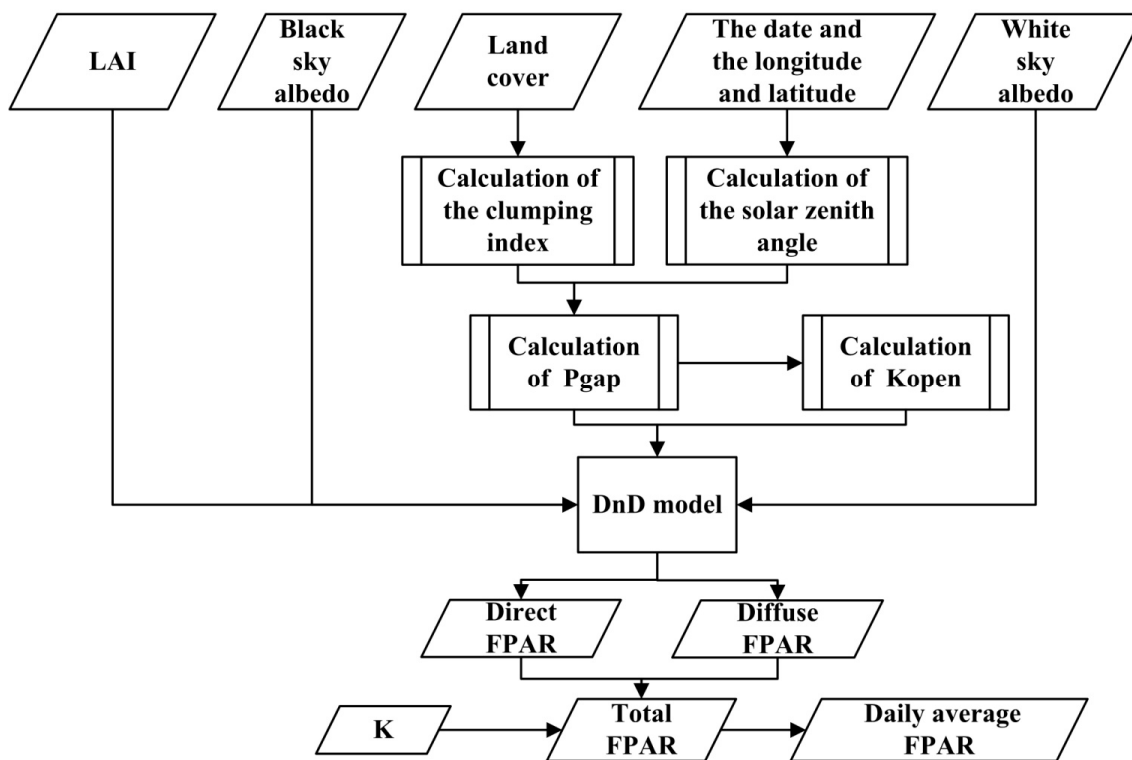


**Figure 1.** Flowchart of *FPAR* inversion.

The solar zenith angle is a function of date, longitude and latitude. It can be calculated using Equation (21):

$$\cos \theta_0 = \sin \delta \sin \phi + \cos \delta \cos \phi \cos \omega \tag{21}$$

where  $\delta$  is the solar declination,  $\Phi$  is the latitude and  $\omega$  is the hour angle. Using this formula, the solar zenith angle can be calculated for the any latitude and time.

The foliage clumping index is closely related to vegetation type. This paper uses the clumping index from Chen’s method [30]. Average clumping indices for different vegetation types are shown in Table 1. The project coefficient *G* is treated as a constant of 0.5 for a spherical distribution of foliage inclination angle [28]. The coefficient *a* is calculated by SAIL model simulation [26]. By inputting the observed leaf reflectance, leaf transmittance and soil reflectance, according to the Equation (7), the

$\alpha_{L-dir}$  and  $\alpha_{L-diff}$  can be simulated with changeable LAI and solar zenith angle. In this paper,  $\alpha_{dir}$  and  $\alpha_{diff}$  are treated as constants with values of 0.96 and 0.93, which are the average of the simulated data.

**Table 1.** Clumping indices for different vegetation types.

Vegetation Type	Clumping Index	Vegetation Type	Clumping Index
Broadleaf, evergreen	0.63	Shrubs	0.71
Broadleaf, deciduous	0.69	Herbaceous	0.74
Needleleaf, evergreen	0.62	Sparse shrubs	0.75
Needleleaf, deciduous	0.68	Cultivated and managed area	0.73
Mixed leaf types	0.69	Other	0.87

### 3. Study Area and Data

The study area is located in the Zhangye area of Gansu Province, China. The Zhangye area is in the midstream zone of the Heihe River Basin (Figure 2). The study area includes various land-cover types, such as desert, cropland, oases, urban areas and mountainous regions. In 2007, an automatic weather station was established by the Institute of Remote Sensing Applications and the Cold and Arid Regions Environmental and Engineering Research Institute, Chinese Academy of Sciences, in the Yingke district of Zhangye City to perform observations of micrometeorology and evapotranspiration [31–33]. Through numerous simultaneous airborne, satellite-borne and ground-based remote-sensing experiments carried out in 2008, a large amount of experimental data of the topography, land cover and other attributes of this area was retrieved. This experiment was repeated in 2012, at which time the authors carried out ground observations of FPAR on maize canopy, alfalfa and grassland. Many PAR quantum sensors were also installed to observe PAR automatically.

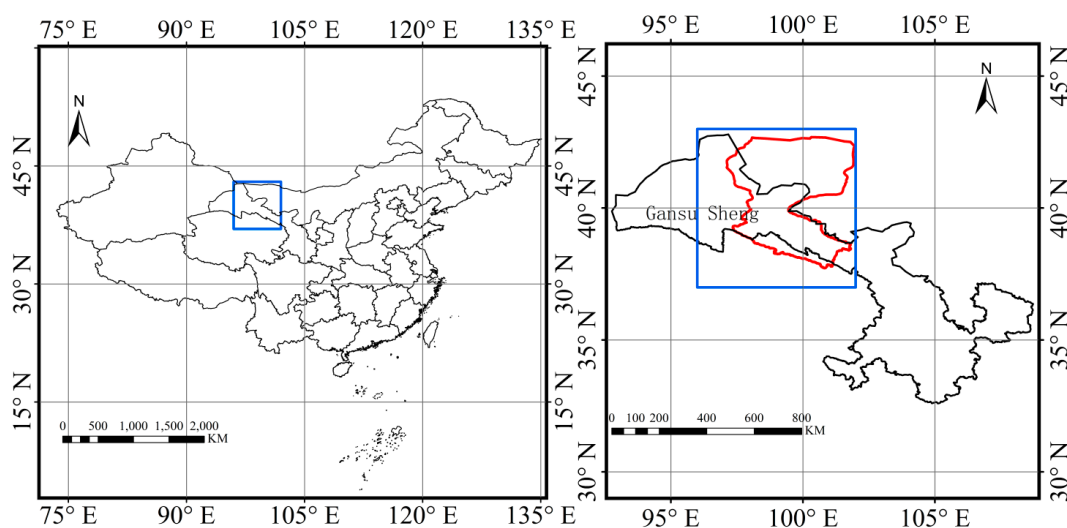


**Figure 2.** Location of the study area. The black-bordered area is Gansu Province; the red-bordered area is the Heihe River Basin; and the blue-bordered area is the region covered by the remote sensing images used for FPAR inversion in this paper.

Use of remote sensing data is the best way for FPAR inversion for the whole Heihe River Basin. Based on the input parameters required by the DnD model, the combined Terra and Aqua MODIS LAI

product (MCD15), surface albedo product (MCD43) and land cover product (MCD12) were used. The diffuse PAR proportion is a by-product of PAR estimation. The authors have developed a method for estimating hourly PAR based on a combination of geostationary and polar-orbiting satellite data [34–36]. The Multifunctional Transport Satellite (MTSAT) was selected to retrieve cloud optical depth (COD) at high temporal resolution, and the polar orbit satellite data of the MODIS products were used to derive surface parameters based on multispectral characteristics. Instantaneous direct and total PAR were estimated by the Second Simulation of a Satellite Signal in the Solar Spectrum-Vector (6SV) and the Santa Barbara DISORT Atmospheric Radiative Transfer (SBDART) model [37,38]. Then, instantaneous  $k$  could be calculated using direct and total PAR. The information of the input data is showed in Table 2.

**Table 2.** Input data for FPAR inversion.

Parameter	Product	Spatial Resolution	Temporal Resolution
LAI	MCD15	1 km	4 days
Black-sky albedo	MCD43	1 km	16 days
White-sky albedo	MCD43	1 km	16 days
Land cover	MCD12	1 km	Yearly
$k$	Calculated by direct and total PAR	1 km	Hourly

The SunScan canopy analysis system can obtain vegetation canopy FPAR. It offers convenient and flexible tools for measuring and analyzing incident and transmitted PAR in crop canopies. It provides vital information about the penetration of PAR into crops and is essential in work, such as comparative crop studies, for separating out the effects of cultivar and treatment. It is particularly well suited to low regular canopies (as found in many agricultural crops). The principle of SunScan measurement of canopy FPAR is shown in Figure 3.

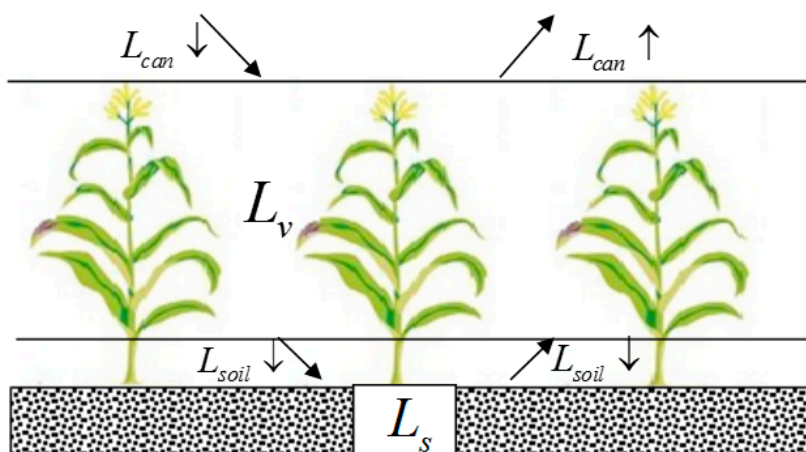


**Figure 3.** Schematic of the SunScan canopy analysis system.

In Figure 3,  $L_{can}\uparrow$  is the PAR that reaches the top of the vegetation canopy,  $L_{can}\downarrow$  is the reflective PAR of the vegetation canopy,  $L_{soil}\uparrow$  is the reflective PAR of the soil and  $L_{soil}\downarrow$  is the PAR that reaches the soil. These four parameters can be obtained from SunScan measurements.  $L_s$  is the absorptive PAR of soil, and  $L_v$  is the absorptive PAR of the vegetation canopy.  $L_s$  and  $L_v$  can be calculated using Equations (22) and (23):

$$L_{can} \downarrow = L_v + L_{can} \uparrow + L_s \quad (22)$$

$$L_s = L_{soil} \downarrow - L_{soil} \uparrow \quad (23)$$

Then, the vegetation canopy FPAR can be expressed as Equation (24):

$$FPAR = \frac{L_v}{L_{can} \downarrow} \quad (24)$$

Long time observation are helpful in obtaining measured canopy FPAR data under different weather conditions and at different times and is also important for the analysis of FPAR characteristics. However, using the SunScan canopy analysis system to obtain a long time of canopy FPAR is time consuming and laborious. The PAR Quantum Sensor is designed to provide accurate, continuous PAR measurements. Therefore, upward and downward photon flux sensors (PQS1) were erected on crop, forest and meadow land surfaces (Figure 4) in the Heihe River Basin. The sensors can observe upward PAR (PAR $\uparrow$ ) and downward PAR (PAR $\downarrow$ ):

$$PAR \downarrow - PAR \uparrow = APAR_{plant} + APAR_{soil} \quad (25)$$

$$APAR_{plant} = FPAR_{plant} \times PAR \downarrow \quad (26)$$

where  $APAR_{plant}$  is the PAR absorbed by the plant canopy and  $APAR_{soil}$  is the PAR absorbed by the soil background. These observed  $APAR$  data were used as indirect validation data for the DnD model.

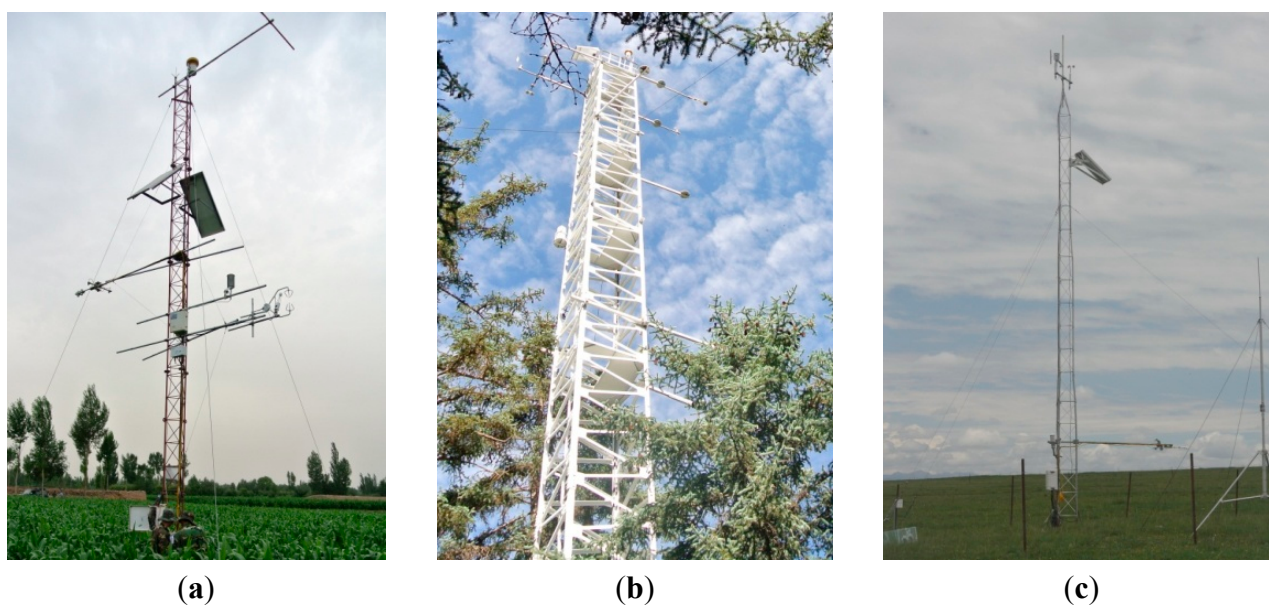


**Figure 4.** PAR observation stations in the Heihe River Basin. (a) The underlying surface is crop; (b) the underlying surface is forest; (c) the underlying surface is meadow.

#### 4. Results and Discussion

With the MODIS products as the primary data input, 12 months of FPAR data in Heihe River Basin were produced, including instantaneous and daily products from 1 January–30 December 2012. The spatial resolution was 1 km. Instantaneous retrieval direct, diffuse and daily average FPAR are shown in Figure 5. This paper analyzes the inversion accuracy of the DnD model from three aspects.

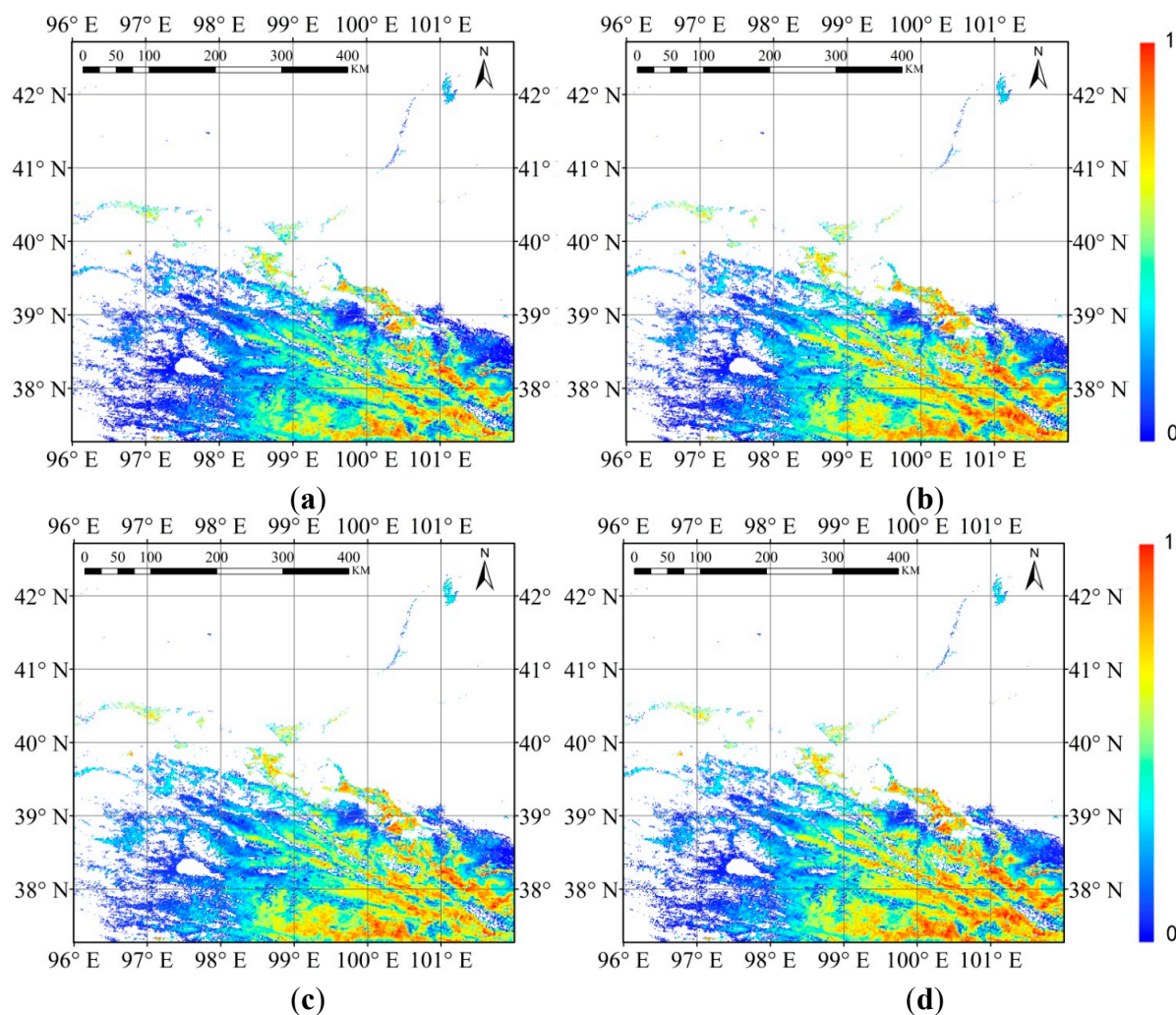


**Figure 5.** FPAR inversion: (a) direct FPAR at noon, 5 July 2012; (b) diffuse FPAR at noon, 5 July 2012; (c) total FPAR at noon, 5 July 2012; (d) daily average FPAR on 5 July 2012.

#### 4.1. Validation with Observed FPAR

To the south of Zhangye City, Gansu Province, large areas of maize have been planted. Its diurnal FPAR changes were observed by the SunScan canopy analysis system on 5 July 2012. Figure 6a shows the difference between observed diurnal FPAR and inversion diurnal FPAR. Both the observational and inversion curves show that FPAR is the highest in the morning and reaching a wave trough around noon. This occurs because the increase in the solar zenith angle makes the light path through the vegetation canopy longer, leading to an increase in FPAR. There are many reasons for uncertainty in the observation process, such as occlusion by leaves, meaning that the observed FPAR curve fluctuates significantly. The spatial resolution of the FPAR inversion is 1 km; the small changes at leaf scale cannot be reflected. The inversion is relatively stable. The observed daily average FPAR was 0.81, and the daily average inverted FPAR was 0.82. This shows that the DnD model can represent the diurnal changes in FPAR and that the daily average value is very close to the observed value. This paper also compared the instantaneous observed and inverted FPAR during July 2012 (Figure 6b). The RMSE was 0.03, and the  $R^2$  was 0.85.

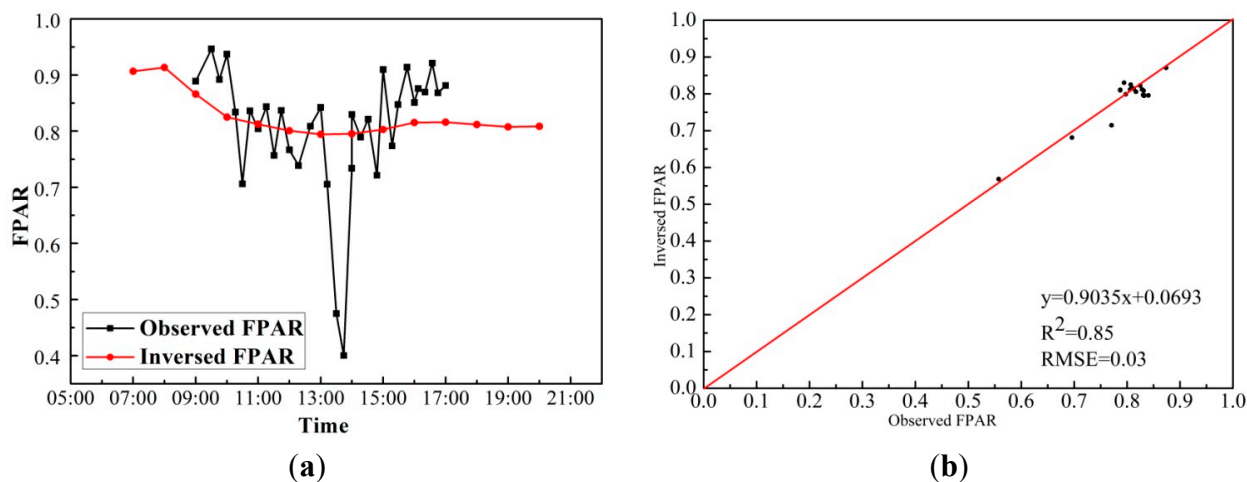


**Figure 6.** Comparison of observed and inversed FPAR: (a) diurnal change curves for observed and inversed FPAR; (b) scatterplots between observed and inversed FPAR.

#### 4.2. Validation with Simulated FPAR by the SAIL Model

Because of the limitations of the measured data, simulated data were used to express the difference between the DnD model and Chen's model. Because Chen's model (without distinguishing direct and diffuse PAR) and the DnD model were developed according to the principle of the energy budget balance, the contrast was focused on these two models. The SAIL model added the 6S atmospheric radiative transfer model, so it is able to reflect the change of FPAR caused by the change of the proportion of the diffuse PAR. Thus, the SAIL model is considered as a standard radiative transfer model. The expression capability of the vegetation radiative transfer model for the DnD model and Chen's model can be performed under different visibility, LAI and solar zenith angle conditions. The SAIL model was used to simulate direct, diffuse and total FPAR under different weather conditions. By changing the input parameters (solar zenith angle, LAI and visibility) of the SAIL model, simulated FPAR values could be obtained. With a solar zenith angle step of  $25^\circ$  and a visibility step of 30 km, FPAR values were calculated for various values of LAI using the DnD model and Chen's model. The differences among the three models are shown in Figure 7. The values simulated by the SAIL model were lower than those given by the other two models. The differences between these three kinds of FPAR gradually decreased with increasing LAI. The relative error between the SAIL and DnD models ranged from 11% to 0.3%, with an RMSE of 0.04. The relative error between the SAIL model and Chen's model ranged from 15% to 0.5%, with in RMSE of 0.05.

In this research, the differences among the three models under various visibility conditions were also analyzed. With an LAI of three and a visibility of 30 km, the relative error between the DnD and SAIL models was 5.4%; the relative error between Chen's model and the SAIL model was 7.2%. With a visibility of 15 km, the relative error between the DnD and SAIL models was 4.3%; the relative error between Chen's model and the SAIL model was 6.6%. With a visibility of 5 km, the relative error between the DnD and SAIL models was 1%; the relative error between Chen's model and the SAIL model was 4.6%. This means that the higher the proportion of diffuse PAR, the closer the value simulated by the DnD model will be to that simulated by the SAIL model, with obviously better accuracy than models that do not distinguish between direct and diffuse FPAR.

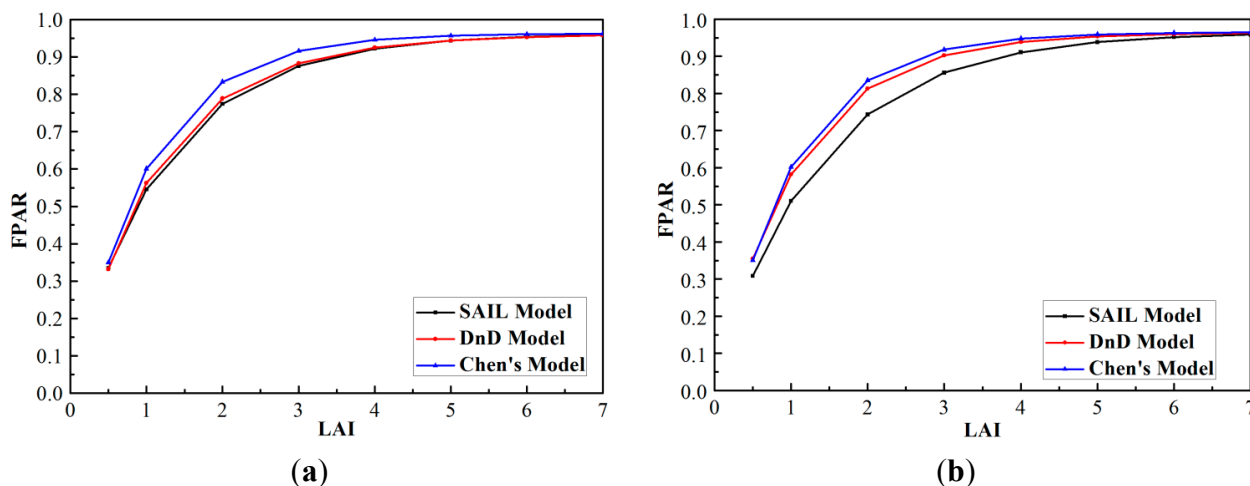


**Figure 7.** Differences among the three kinds of models based on simulated data: (a) with visibility of 5 km; (b) with visibility of 30 km. SAIL, scattering by arbitrarily-inclined leaves; DnD, direct and diffuse radiation.

4.3. Validation with Observed PAR Data

Figure 8 shows the differences between observed and inversed APAR. The observed APAR is the sum of vegetation canopy absorption PAR and soil absorption PAR; inversed APAR includes only vegetation canopy absorption PAR. Therefore, the observed APAR should be larger than the inversed value. In the period of vegetation ridge covered, the vegetation FPAR was larger, and the two APAR values were close to each other. However, when FPAR was smaller, the difference between the two APAR values was relatively larger. This occurred because the contribution of soil absorption PAR increased. Therefore, if precise verification of vegetation absorption PAR using observed APAR data is needed, the soil absorption part must be removed. This kind of observed data is obtained in the period of the vegetation ridge covered.

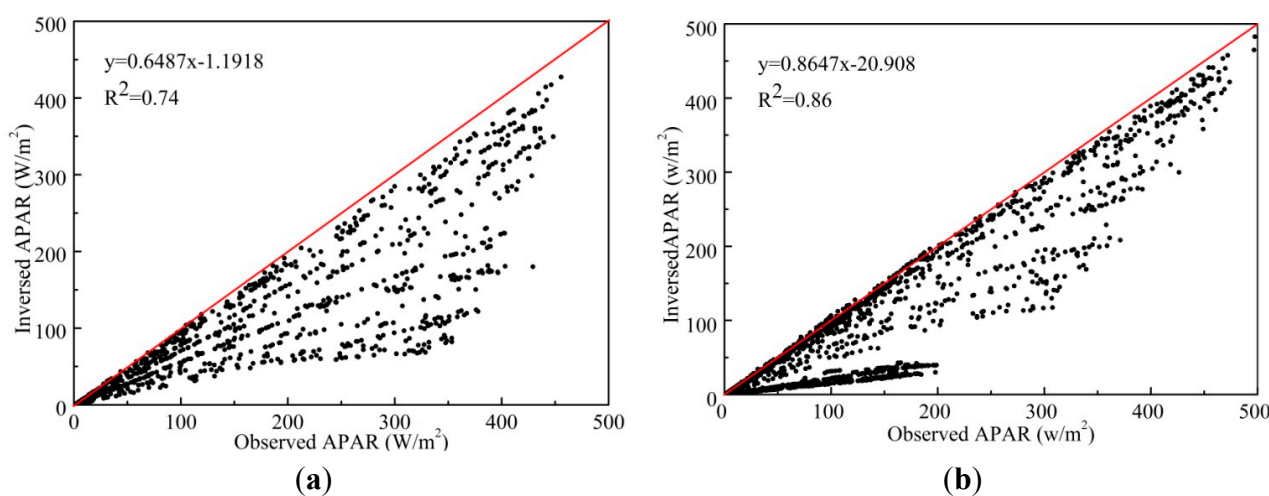


**Figure 8.** Scatterplots of inversed and observed APAR with an underlying surface of: (a) cropland; (b) meadowland.

4.4. Validation with the MODIS FPAR Product

The MODIS FPAR product is primary data input for calculating GPP. In this paper, the MODIS LAI product was used as an important input to calculate FPAR. Therefore, for various vegetation types, a comparative analysis of the MODIS FPAR product and the FPAR product calculated in this research was performed (Figure 9). Because the MODIS LAI and surface albedo products were used to calculate FPAR in this study, the inversion results and the MODIS FPAR product were highly correlated. Values from the MODIS FPAR product were higher than those from the inversion product, but the biggest RMSE was 0.06 for the evergreen needleleaf vegetation type. Many previous studies have pointed out the accuracy of the MODIS FPAR product. McCallum *et al.* compared four global FPAR datasets over northern Eurasia for 2000, namely MODIS, CYCLOPES (Carbon Cycle and Change in Land Observational Products from an Ensemble of Satellites), JRC (Joint Research Center) and GLOBCARBON [39]. The results showed that both the MODIS and CYCLOPES datasets recorded on average similar, but substantially higher values than the JRC and GLOBCARBON datasets. Fensholt *et al.* compared MODIS FPAR data with site-measured data [40]. The MODIS FPAR values were overestimated by 0.06–0.15 (approximately 8%–20%). Pinty *et al.* examined MODIS and JRC FPAR products over a site in eastern Russia. MODIS grossly overestimated the values for deciduous needleleaf larch forest [41]. These conclusions are consistent with the comparison results reported above.

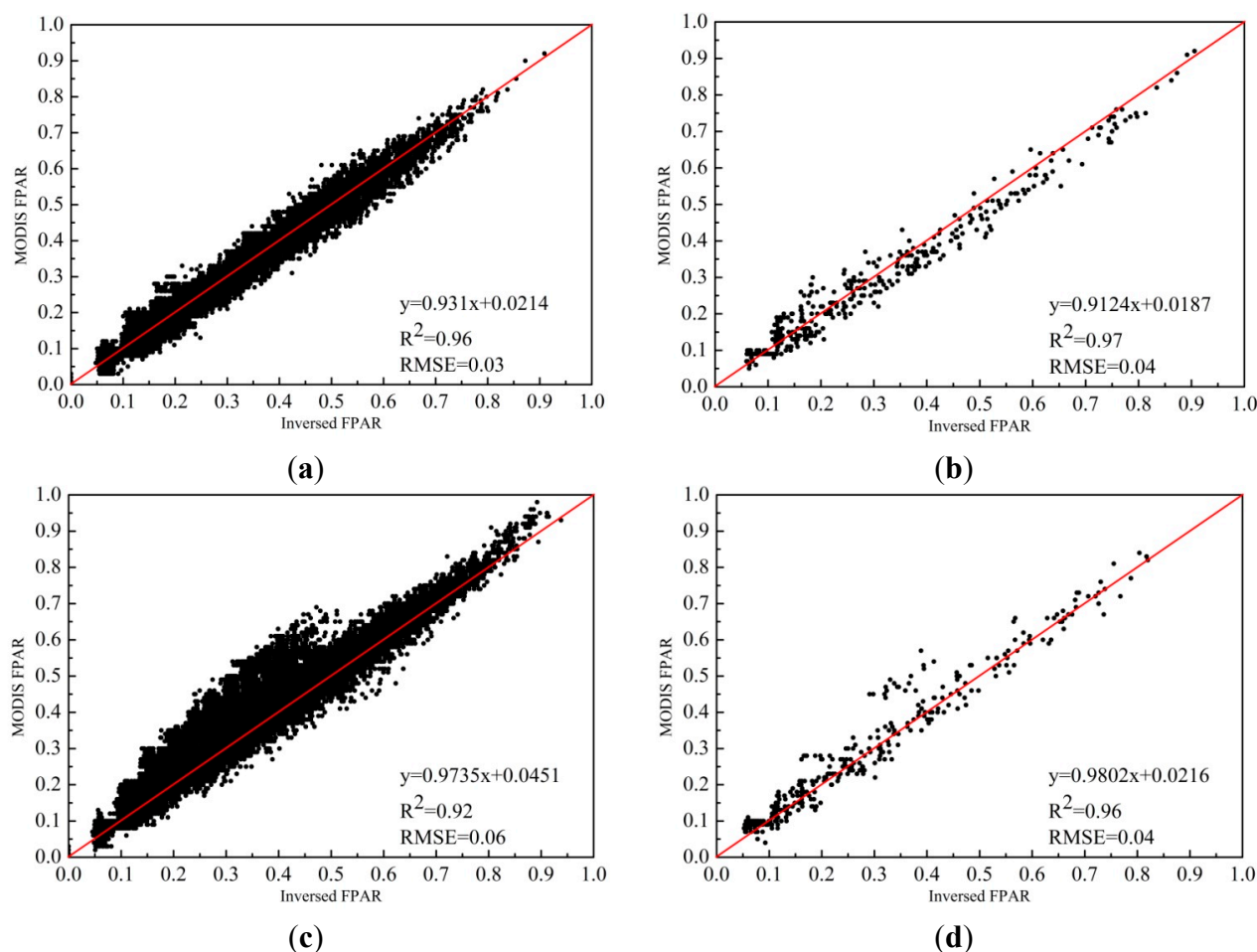


**Figure 9.** Scatterplots of inversion FPAR and MODIS FPAR for various vegetation types: (a) shrubs; (b) herbaceous; (c) evergreen needleleaf; (d) deciduous needleleaf.

For the comparison of the variability of the inversed FPAR by the DnD model and the MODIS FPAR product, a method for the comparison of three kinds of multitemporal FPAR products in a previous study was used. The agreement coefficient (AC) was calculated, and the spatial agreement and temporal agreement were analyzed. AC is used to assess the agreement between two images, non-dimensional, bounded (0–1 for no to perfect agreement) and symmetric (no preference for one dataset).  $AC = 1 - (SSD/SPOD)$ , where  $SSD$  is the sum of squared differences and  $SPOD$  is the sum of potential differences [42]:

$$SSD = \sum_{i=1}^n (X_i - Y_i)^2, SPOD = \sum_{i=1}^n (|\bar{X} - \bar{Y}| + |X_i - \bar{X}|)(|\bar{X} - \bar{Y}| + |Y_i - \bar{Y}|) \quad (27)$$

To be able to compare, the total daily inversed FPAR in the Heihe River Basin was averaged for eight days. The analysis is performed on the full year of 2012. The analysis of the temporal evolution of selected spatial metrics aims to highlight specific periods of spatial disagreement [42]. As an example, Figure 10 shows the mean FPAR and the temporal profile of AC between paired datasets for the shrub and evergreen needleleaf forest land cover.

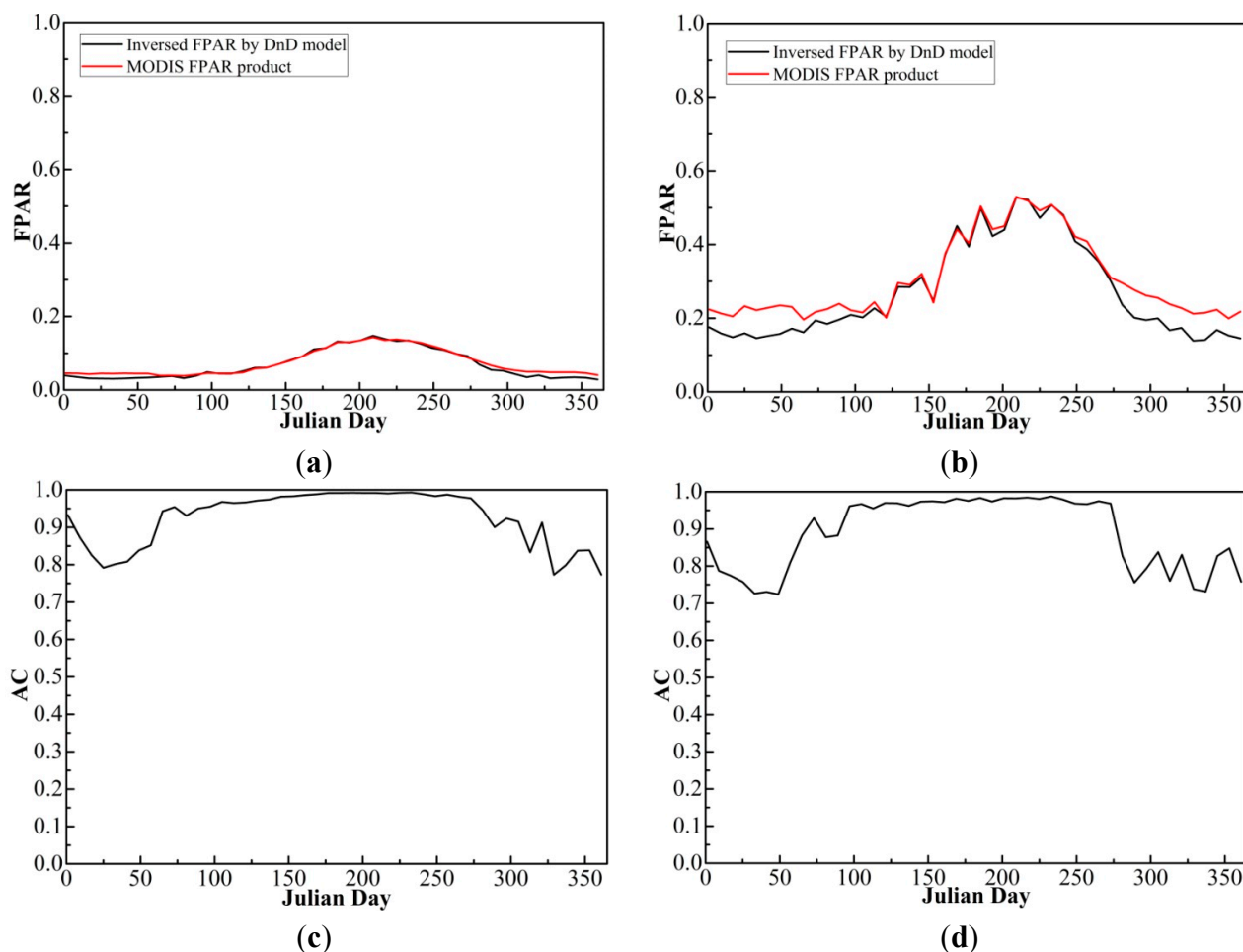


**Figure 10.** Temporal profiles of shrub and evergreen needleleaf forest land cover classes over the Heihe River Basin. (a) mean FPAR values of inversed FPAR by the DnD model and the MODIS FPAR product of shrub land cover; (b) mean FPAR values of inversed FPAR by the DnD model and the MODIS FPAR product of evergreen needleleaf forest land cover; (c) agreement coefficient (AC) of shrub land cover; (d) AC of needleleaf forest land cover.

Same as the mean of FPAR, AC also has seasonality for the shrub and needleleaf forest land cover. There is minimum agreement between inversed FPAR and the MODIS FPAR product in wintertime (November to February). When the FPAR value becomes smaller, the AC between two datasets is smaller. The MODIS FPAR is higher than inversed FPAR, especially in wintertime for the forest land cover (Figure 10a,b). This shows the difference between the DnD model and MODIS FPAR method. In winter, vegetation is sparse; there is a greater chance of direct light passing through the vegetation to reach the land surface. The impact of changes in the diffuse PAR proportion to the total FPAR is more obvious. In summer, the FPAR approaches saturation, and the difference between the two algorithms is also smaller.

Figure 11 shows the the temporal AC for Heihe River Basin. A high agreement is found in the southern part of the region, where vegetation has a distinct seasonality. Otherwise, in the northern part of the region, there is a low temporal correlation between the two datasets for the desert and Gobi land cover. The FPAR value is zero or very low for the whole year.

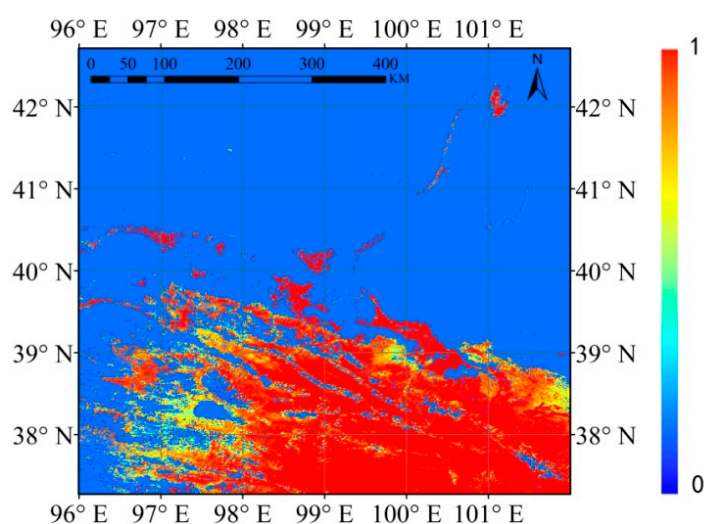


**Figure 11.** Map of the temporal AC for Heihe River Basin.

## 5. Conclusions

In this paper, an FPAR inversion model (the DnD model), which distinguishes direct and diffuse radiation, was proposed based on the energy budget balance theory. Because of the different transmission processes of direct and diffuse skylight in the vegetation canopy, the DnD model has different solutions for these two cases. Instantaneous FPAR at any given time can be calculated through different solar zenith angles and diffuse PAR proportion inputs. On the assumption that LAI and surface albedo do not change over short periods, FPAR on a cloudy day can also be obtained from the DnD model. From a comparative analysis of the DnD model with models that do not distinguish direct and diffuse radiation, the diffuse PAR proportion was found to be larger in the FPAR calculated by the DnD model and closer to the SAIL model simulation results than those from the other kind of model. This shows that the DnD model has good performance under cloudy sky.

Therefore, this method can improve the temporal resolution of FPAR products. To validate the accuracy of the DnD model, direct, diffuse and total FPAR for 2012 in the Heihe River Basin were inversed. Instantaneous FPAR was validated by measured FPAR and measured APAR. The RMSE

between inversed and measured FPAR is 0.03;  $R^2$  is 0.85. In this paper, diurnal changes in instantaneous inversion FPAR were also compared with measured diurnal change data. It could be concluded that the characteristics of diurnal change in FPAR can be expressed by the DnD model. Daily average FPAR was validated by the MODIS FPAR product. The inversion results and the MODIS FPAR product were found to be highly correlated, but the MODIS FPAR product slightly overestimated FPAR in forest areas. The inversed FPAR was closer to the true value. Through producing the regional FPAR products in a year and validation with the observation data and other FPAR products, the uncertainty and accuracy of this model were clearly demonstrated. This improvement is very helpful in calculating GPP. Because the model formulas are easy to implement, they are highly suitable for integration into production systems to generate regional FPAR datasets.

All of these analyses showed that the difference between direct and diffuse FPAR cannot be ignored. The inversion model used in this research was helpful in improving FPAR inversion accuracy. However, the DnD model has certain limitations. The input parameters include LAI, surface albedo, land cover and diffuse PAR proportion. The precision of these parameters directly affects the accuracy of FPAR inversion. In addition, many unanswered questions remain to be studied, such as multiple scattering of the soil background, acquisition of observed FPAR data and removal of the absorption PAR of soil from observed APAR.

### **Acknowledgments**

This work was jointly supported by the Key Deployment Project of the Chinese Academy of Sciences (KZCX2-XB3-15-2), the Chinese Natural Science Foundation (Project 41101324), the State Key Laboratory of Remote Sensing Science (Project 13RC-02) and the National High-Technology Research and Development Program of China (Project 863: 2012AA12A304). Thanks to Wenjie Fan from Peking University for joint FPAR ground observations. Thanks also to Xin Li, Mingguo Ma and Junlei Tan from the Cold and Arid Regions Environment and Engineering Research Institute, Chinese Academy of Sciences, for support with photon flux sensor erection in the Heihe River Basin.

### **Author Contributions**

Li Li constructed the model, performed the FPAR inversion, analyzed the results and wrote the paper. Yongming Du was involved mainly in model construction. Yong Tang's contribution was the FPAR simulation using the SAIL model. Xiaozhou Xin directed the field work. Hailong Zhang was responsible for calculating the proportions of diffuse skylight. Jianguang Wen was responsible for the inversion of surface albedo. Qinhua Liu is the corresponding author and pointed out the problem of distinguishing between direct and diffuse FPAR.

### **Conflicts of Interest**

The authors declare no conflict of interest.

## References

1. Myneni, R.B.; Knyazikhin, Y.; Privette, J.L.; Glassy, J.; Tian, Y.; Lotsch, A.; Zhang, Y.; Wang, Y.; Morisette, J.T.; Votava, P.; *et al.* MODIS Leaf Area Index (LAI) and Fraction of Photosynthetically Active Radiation Absorbed By vegetation (FPAR) Product (MOD15). 1999. Algorithm Theoretical Basis Document Version 4.0. Available online: <http://modis-land.gsfc.nasa.gov/lai.html> (accessed on 18 May 2015).
2. Deering, D.W. *Rangeland Reflectance Characteristics Measured by Aircraft and Spacecraft Sensors*; Texas A & M University: College Station, TX, USA, 1978.
3. Huete, A.R.; Liu, H.Q.; Batchily, K.; van Leeuwen, W. A comparison of vegetation indices over a global set of TM images for EOS-MODIS. *Remote Sens. Environ.* **1997**, *59*, 440–451.
4. Goward, S.N.; Huemmrich, K.F. Vegetation canopy PAR absorptance and the normalized difference vegetation index: An assessment using the SAIL model. *Remote Sens. Environ.* **1992**, *39*, 119–140.
5. Sellers, P.J. Canopy reflectance, photosynthesis and transpiration. *Int. J. Remote Sens.* **1985**, *6*, 1335–1372.
6. Sellers, P.J.; Los, S.O.; Tucher, C.J.; Collatz, G.J.; Justice, C.O.; Dazlich, D.A.; Randall, D.A. A global  $1 \times 1$  NDVI data set for climate studies. Part 2: The generation of global fields of terrestrial biophysical parameters from the NDVI. *Int. J. Remote Sens.* **1994**, *15*, 3519–3545.
7. Xiao, X.M.; Hollinger, D.; Aber, J.; Goltz, M.; Davidson, E.A.; Zhang, Q.; Moore, B., III. Satellite-based modeling of gross primary production in an evergreen needle leaf forest. *Remote Sens. Environ.* **2004**, *89*, 519–534.
8. Xiao, X.M.; Zhang, Q.; Braswell, B.; Urbanski, S.; Boles, S.; Wofsy, S.; Moore, B., III; Ojima, D. Modeling gross primary production of temperate deciduous broadleaf forest using satellite images and climate data. *Remote Sens. Environ.* **2004**, *91*, 256–270.
9. Roujean, J.L.; Breon, F.M. Estimating PAR absorbed by vegetation from bidirectional reflectance measurements. *Remote Sens. Environ.* **1995**, *51*, 375–384.
10. Dawson, T.P.; North, P.R.J.; Plummer, S.E.; Curran, P.J. Forest ecosystem chlorophyll, content: Implications for remotely sensed estimates of net primary productivity. *Int. J. Remote Sens.* **2003**, *24*, 611–617.
11. Chen, L.F.; Gao, Y.H.; Li, L.; Liu, Q.; Gu, X. Forest NPP estimation based on MODIS data under cloudless condition. *Sci. China Ser. D Earth Sci.* **2008**, *51*, 331–338.
12. Tao, X. Remote Sensing Retrieval of FAPAR: Model and Scaling Effect. Master's Thesis, Peking University, Beijing, China, 2009.
13. Fan, W.J.; Liu, Y.; Xu, X.R.; Chen, G.; Zhang, B. A new FAPAR analytical model based on the law of energy conservation: A case study in China. *IEEE J. Sel. Top. Appl. Earth Obs. Remote Sens.* **2014**, *99*, doi:10.1109/JSTARS.2014.2325673.
14. Roderick, M.L.; Farquhar, G.D.; Berry, S.L.; Noble, L.R. On the direct effect of clouds and atmospheric particles on the productivity and structure of vegetation. *Oecologia* **2001**, *129*, 21–30.

15. Yamasoe, M.A.; Von, R.C.; Manzi, A.O.; Schafer, J.S.; Eck, T.F.; Holben, B.N. Effect of smoke and clouds on the transmissivity of Photosynthetically active radiation inside the canopy. *Atmos. Chem. Phys.* **2006**, *6*, 1645–1656.
16. Gu, L.H.; Baldocchi, D.D.; Wofsy, S.; Munger, J.W.; Michalsky, J.J.; Urbanski, S.P.; Boden, T.A. Response of a deciduous forest to the Mount Pinatubo eruption: Enhanced photosynthesis. *Science* **2003**, *299*, 2035–2038.
17. Farquhar, G.D.; Roderick, M.L. Pinatubo, Diffuse Light, and the Carbon Cycle. *Science* **2003**, *299*, 1997–1998.
18. Mercado, L.M.; Bellouin, N.; Sitch, S.; Boucher, O.; Huntingford, C.; Wild, M.; Cox, P.M. Impact of changes in diffuse radiation on the global land carbon sink. *Nature*. **2009**, *458*, 1014–1018.
19. He, X.Z.; Zhou, T.; Jia, G.S.; Zhang, Z.Y.; Li, X.J.; Zhao, C.; Feng, S.H. Modeled effects of changes in the amount and Diffuse Fraction of PAR on Forest GPP. *J. Nat. Resour.* **2011**, *26*, 619–634.
20. Baret, F.; Guyot, G. Potentials and limits of vegetation indices for LAI and PAR assessment. *Remote Sens. Environ.* **1991**, *35*, 161–173.
21. Zhou, B. The study of Fraction of Photosynthetic Active Radiation using Monte Carlo method. Master's Thesis, Institute of Remote Sensing Applications, Chinese Academy of Science, Beijing, China, 2007.
22. Suits, G.H. The calculation of the directional reflectance of a vegetative canopy. *Remote Sens. Environ.* **1972**, *2*, 117–125.
23. Verhoef, W. Light scattering by leaf layers with application to canopy reflectance modeling: The SAIL model. *Remote Sens. Environ.* **1984**, *16*, 125–141.
24. Verhoef, W. Earth observation modeling based on layer scattering matrices. *Remote Sens. Environ.* **1985**, *17*, 165–178.
25. Goel, N.S.; Strelbel, D.E. Simple beta distribution representation of leaf orientation in vegetation canopies. *Agron. J.* **1984**, *76*, 800–803.
26. Li, L.; Fan, W.J.; Du, Y.M.; Tang, Y.; Xin, X.Z.; Zhang, H.L.; Liu, Q.H. A Characteristic Study of Crop Canopy Direct and Diffuse Fraction of Absorbed Photosynthetically Active Radiation Based on SAIL Model Simulation. *Acta Sci. Nat. Univ. Pekin.* **2015**, *51*, 99–108.
27. Li, W.J.; Fang, H.L. Estimation of direct, diffuse, and total FPARs from Landsat surface reflectance data and ground-based estimates over six FLUXNET sites. *J. Geophys. Res. Biogeosci.* **2015**, *120*, doi:10.1002/2014JG002754.
28. Chen, J.M. Canopy architecture and remote sensing of the fraction of photosynthetically active radiation absorbed by boreal conifer forest. *IEEE Trans. Geosci. Remote Sens.* **1996**, *34*, 1353–1368.
29. Li, X.W.; Wang, J.D. *Vegetation Optical Remote Sensing Model and Parameterized Vegetation Structure*; Science Press: Beijing, China, 1995. (in Chinese)
30. Chen, J.M.; Menges, C.H.; Leblanc, S.G. Global mapping of foliage clumping index using multi-angular satellite data. *Remote Sens. Environ.* **2005**, *97*, 447–457.
31. Li, X.; Li, X.W.; Li, Z.Y.; Ma, M.G.; Wang, J.; Xiao, Q.; Liu, Q.; Che, T.; Chen, E.X.; Yan, G.J.; *et al.* Watershed allied telemetry experimental research. *J. Geophys. Res.* **2009**, *114*, doi:10.1029/2008JD011590.

32. Li, X.; Cheng, G.D.; Liu, S.M.; Xiao, Q.; Ma, M.G.; Jin, R.; Che, T.; Liu, Q.H.; Wang, W.Z.; Qi, Y., *et al.* Heihe Watershed Allied Telemetry Experimental Research (HiWATER): Scientific objectives and experimental design. *Bull. Am. Meteorol. Soc.* **2013**, *94*, 1145–1160.
33. Cheng, G.D.; Li, X.; Zhao, W.Z.; Xu, Z.M.; Feng, Q.; Xiao, S.C.; Xiao, H.L. Integrated study of the water-ecosystem-economy in the Heihe River Basin. *Nat. Sci. Rev.*, **2014**, *1*, 413–428.
34. Li, L.; Xin, X.Z.; Su, G.L.; Liu, Q.H. Photosynthetically active radiation retrieval based on HJ-1A/B satellite data. *Sci. China Earth Sci.* **2010**, *53*, 81–91.
35. Li, L. PAR and FPAR Retrieval Base on Multi-Source Remote Sensing Data. Ph.D. Thesis, Institute of Remote Sensing Applications, Chinese Academy of Science, Beijing, China, 2010.
36. Zhang, H.; Xin, X.; Li, L.; Liu, Q. An improved parametric model for simulating cloudy sky daily direct solar radiation. *IEEE J. Sel. Top. Appl. Earth Obs. Remote Sens.* **2013**, *6*, 180–187.
37. Vermote, E.F.; Tanré, D.; Deuze, J.L.; Herman, M.; Morcette, J.J. Second simulation of the satellite signal in the solar spectrum, 6S: An overview. *IEEE Trans. Geosci. Remote Sens.* **1997**, *35*, 675–686.
38. Ricchiazzi, P.; Yang, S.; Gautier, C.; Sowle, D. SBDART: A research and teaching software tool for plane-parallel radiative transfer in the Earth's atmosphere. *Bull. Am. Meteorol. Soc.* **1998**, *79*, 2101–2114.
39. McCallum, L.; Wagner, W.; Schmullius, C.; Shvidenko, A.; Obersteiner, M.; Fritz, S.; Nilsson, S. Comparison of four global FAPAR datasets over Northern Eurasia for the year 2000. *Remote Sens. Environ.* **2010**, *114*, 941–949.
40. Fensholt, R.; Sandholt, I.; Rasmussen, M.S. Evaluation of MODIS LAI, fAPAR and the relation between fAPAR and NDVI in a semi-arid environment using *in situ* measurements. *Remote Sens. Environ.* **2004**, *91*, 490–507.
41. Pinty, B.; Lavergne, T.; Kaminski, T.; Aussedat, O.; Giering, R.; Gobron, N.; Taberner, M.; Verstraete, M.M.; Voßbeck, M.; Widlowski, J.-L.; *et al.* Partitioning the solar radiant fluxes in forest canopies in the presence of snow. *J. Geophys. Res.* **2008**, *113*, doi:10.1029/2007JD009096.
42. Meroni, M.; Atzberger, C.; Vancutsem, C.; Gobron, N.; Baret, F.; Lacaze, R.; Eerens, H.; Leo, O. Evaluation of agreement between space remote sensing SPOT-VEGETATION fapar time series. *IEEE Trans. Geosci. Remote Sens.* **2013**, *51*, 1951–1962.